1 **Effect of ball-milling on crystallinity index, degree of polymerization and thermal stability**

2 **of cellulose:** ~~a systematic study~~

3 Marco Mattonai[a], Dominika Pawcenis[b], Serena del Seppia[a], Joanna Łojewska[b], Erika

4 Ribechini[a]*

5 [a]Department of Chemistry and Industrial Chemistry, University of Pisa, Via G. Moruzzi 13,

6 56124 Pisa, Italy

7 [b]Department of Chemistry, Jagiellonian University, Gronostajowa 2, 30-387 Kraków, Poland

8 *Corresponding Author, erika.ribechini@unipi.it

9

10 **ABSTRACT**

11 A combined study of crystallinity index (CI), degree of polymerisation (DP) and thermal

12 stability of cellulose was carried out for monitoring the effect of ball-milling. DP and CI are

13 two fundamental quantities that describe the physico-chemical behaviour of cellulose. Milling

14 is a common strategy to reduce cellulose crystallinity. In this work, four different

15 commercially available celluloses were milled at 30, 60 and 120 min, and the changes in DP

16 and CI were monitored using spectroscopic, diffraction and chromatographic techniques.

17 Evolved gas analysis-mass spectrometry (EGA-MS) was also used to evaluate the changes in

18 apparent activation energy (E_a) of the pyrolysis reaction upon different milling times by using

19 model-free isoconversional methods. The results showed substantial decrease in CI values

20 and moderate changes in DP after two-hours of ball-milling. E_a were found in the range 110-

21 140 kJ/mol, and were reduced by 10% on average after two hours of ball-milling.

22

25

26

1. INTRODUCTION

Cellulose, the most abundant organic polymer on Earth, is an infinitely surprising material, with application potential in many research fields including renewable energy, material development and medicine (Kian et al., 2018; Lavoine et al., 2012; Qiu & Hu, 2013; Siqueira et al., 2010; Yang et al., 2018). Two main parameters describe the structure of cellulose: the degree of polymerisation (DP), which is the average length of the polysaccharide chains, and the crystallinity index (CI), which is the percentage of crystalline cellulose. The chemical and physico-chemical behaviour of cellulose is deeply influenced by these parameters. Celluloses with high DPs and CIs are more resistant to hydrolysis and show increased density and tensile strength (Bledzki & Gassan, 1999; Hallac & Ragauskas, 2011; Marx-Figini & Maximino, 1993; Schenzel et al., 2005; Siqueira et al., 2010). A recent paper by Mukarakate and co-workers also provides a systematic study of the effect of crystallinity on the thermal stability and products distribution of cellulose allomorphs during pyrolysis (Mukarakate et al., 2016).

The knowledge of DP, CI and thermal stability of a cellulosic material is fundamental for the optimization of its conversion processes, on both the laboratory and the industrial scale. The polymerization degree is usually estimated using viscosimetry or size-exclusion chromatography (SEC) (De Silva & Byrne, 2017; Hallac & Ragauskas, 2011; Łojewski et al., 2010; Ni et al., 2015; Podzimek, 2014; Rebière et al., 2016). SEC analysis with multi-angle light-scattering (MALS) detection constitutes a special case, since this technique provides the so called absolute DP values and requires no calibration with molar mass standards such as polystyrene samples with different hydrodynamic radii (Pawcenis et al., 2015; Podzimek, 2011). The crystallinity index is typically measured by XRD spectroscopy (French & Santiago Cintrón, 2013; Lee & Mani, 2017; Zhao et al., 2017), but reliable estimations can also be

obtained by infrared and Raman-infrared spectroscopy (Agarwal et al., 2010; Schenzel et al., 2005). The thermal stability can be estimated by thermogravimetric analysis (TGA-MS or TGA-FTIR) by using model-free or model-based isoconversional methods. The advantage of model-free isoconversional methods is that no assumptions are made on the thermal degradation mechanism. This allows obtaining meaningful data even for samples with very complex thermal degradation pathways such as cellulose (Ali et al., 2017; Kaur et al., 2018; Sánchez-Jiménez et al., 2011). Recently, model-free isoconversional methods were also applied to evolved gas analysis-mass spectrometry (EGA-MS) (Kim et al., 2017), showing that this technique can provide the same information as TGA.

Milling is a very common strategy to reduce the CI of cellulose (Alvira et al., 2010; da Silva et al., 2010; Gu et al., 2018; Wang et al., 2017). However, it is difficult to find a consensus in the literature regarding the milling time required to eliminate the crystalline phase. Avolio et al. (Avolio et al., 2012) showed that 60 minutes of ball-milling reduce the CI of cellulose from 0.53 to 0.15, but are not sufficient to achieve total amorphization. Schenzel and co-workers (Schenzel et al., 2005) obtained a totally amorphous cellulose after 30 hours of milling, and mixed amorphous and un-milled cellulose to obtain samples at different CIs. A similar strategy was used by Agarwal and co-workers (Agarwal et al., 2010), but totally amorphous cellulose was obtained after only 120 minutes of milling. The paper by Agarwal and co-workers also provides viscosimetric measurements of the DP before and after milling, but the variation is considered as negligible.

In the present work, four commercially available celluloses were milled at 30, 60 and 120 minutes. The effect of ball milling on both the CI and the DP was investigated using ATR-FTIR, XRD and SEC-MALS. EGA-MS was used to calculate the apparent activation energy for the

73 pyrolysis reaction of all the samples by application of model-free isoconversional methods.

74 To the best of our knowledge, this work is a first systematic study of the effects of milling on

75 CI, DP and thermal stability of cellulose using multiple analytical techniques and

76 isoconversional methods.

77

78 ## 2. MATERIALS AND METHODS

79 **2.1 Materials:** Pyridine (≥ 99.9%, Sigma, USA), phenyl-isocyanate (≥ 99.9%, Sigma, USA),

80 methanol (Stanlab, Poland) and tetrahydrofuran (Chempur, Poland) were used for cellulose

81 derivatisation and SEC analyses. Four different cellulose samples were purchased from Sigma,

82 USA: Sigmacell type 20 (labelled "S20", from cotton linters, product n° 310697), Sigmacell

83 type 50 (labelled "S50", from cotton linters, product n° S5504), Microcrystalline cellulose

84 (labelled "SMC", from cotton linters, product n° 435263), and acid-washed cellulose (labelled

85 "SAW", from fir, product n° 22182). All cellulose samples were milled for 30, 60 and 120 min

86 using a Pulverisette 23 ball-mill (Fritsch, Germany).

87

88 **2.2 ATR-FTIR:** Infrared spectra were recorded for all samples in ATR mode using a Nicolet

89 8700 FT-IR spectrometer (Thermo Scientific, USA) and a GladiATR sample holder (PIKE

90 Technologies, USA). The sample holder was equipped with a heating plate, which was kept at

91 105 °C during all measurements to ensure the removal of bound water, which gives the

92 bending vibrational modes at around 1640 cm^{-1}. Spectra were recorded in the range 650–

93 4000 cm^{-1} with a resolution of 4 cm^{-1}. Background spectra were collected before every

94 sample, and all spectra were corrected by subtraction of atmospheric H_2O and CO_2 signals. All

95 spectra were collected in triplicates and averaged. The spectra were processed with OMNIC

96 (Thermo Scientific, USA) and Essential FTIR (Operant LLC, USA). After baseline subtraction,

97 absorbance values were normalized using the area of the C-H stretching band at 2900 cm^{-1}

98 which was used as an internal standard according to the calibration method described by

99 Lojewska et al. (Łojewska et al., 2005). The area was calculated in the range 2700-3000 cm^{-1}.

100 Attribution of the peaks in the IR spectra was based on literature references (Ogundare et al.,

101 2017; Schwanninger et al., 2004; Xu et al., 2013; Zhao et al., 2017).

102

103 **2.3 XRD:** X-ray diffractograms were recorded with a D2-PHASER spectrometer (Bruker, USA).

104 Spectra were recorded in the range 2θ = 4–60 degrees, with a resolution of 0.016 degrees.

105 The CuKα emission at 1.54 Å was used as X-ray source. Cumulative spectra were obtained by

106 recording three diffractograms for each sample. During each measurement, the sample was

107 kept under rotation to prevent iso-orientation effects. The spectra were processed with

108 DIFFRAC (Bruker, USA). Baseline subtraction and peak fitting were performed using PeakFit

109 (Systat Software Inc., USA). Simulated diffraction patterns were used as reference to establish

110 the appropriate number of peaks (French, 2014).

111 Crystallinity indices were evaluated with the peak fitting method (Park et al., 2010), assuming

112 the presence of five Gaussian peaks for the crystalline phase and a sixth Gaussian peak for

113 the amorphous phase. Once the peak areas were calculated from the peak fitting, CI was

114 determined with equation (1), where A_{AM} is the area of the amorphous cellulose peak, and

115 A_{TOT} is the total area of all peaks. The r^2 values for the fitted peaks were always greater than

116 0.95. The dimensions of the crystallites in the un-milled samples were also estimated using

117 the Scherrer equation (2), where τ is the crystallite dimension, K a shape factor which was set

118   to 1.0 (Yue et al., 2015), λ the wavelength of incident light, θ the nominal diffraction angle for

119   a given diffraction peak, and b the half-height width of the peak.

120

121   (1) $CI = 1 - A_{AM}/A_{TOT}$

122   (2) $\tau = K\lambda/bcos\theta$

123

124   **2.4 SEC-UV-MALS-DRI:** Before SEC analysis, all cellulose samples were converted into

125   cellulose tricarbanilate (CTC) with a previously optimised procedure (Pawcenis et al., 2015).

126   Briefly, 5 mg of each sample were weighted in a glass vial and dried at 105 °C for 30 min. The

127   derivatisation was performed by adding 1 mL of pyridine and 0.1 mL of phenyl-isocyanate to

128   the vials, and by keeping the vials at 80 °C for 48 h. After this time, 0.1 mL of methanol were

129   added to stop the reaction. Finally, the solution was diluted with 10 mL of tetrahydrofuran

130   and filtered on 0.45 μm PTFE syringe filters (Equimed, Poland) and injected in the

131   chromatographic system.

132   The SEC apparatus consisted of a 1515 isocratic pump and a 717+ auto-sampler (Waters, USA).

133   Detection was performed using a 2487 UV detector (Waters, USA), Dawn Heleos multi-angle

134   light scattering detector (Wyatt Techology, USA), and Optilab T-rEX differential refractive

135   index detector (Wyatt Technology, USA). The separation was achieved using tetrahydrofuran

136   as mobile phase, and two Jordi Gel DVB columns (25 cm x 1 cm, 500 Å packing, Jordi Labs,

137   USA) equipped with a Styragel guard column (4.6 mm x 30 mm, 20 μm, Waters, USA). The

138   chromatographic columns were kept at 35 °C during all experiments. Mobile flow rate was 1

139   mL min^{-1}, and injection volume was 100 μL. Replicates were made for all samples to evaluate

140   uncertainty. Data elaboration was performed using Astra 6.1.7.17 (Wyatt Technology, USA).

141 SEC analyses provide the weight-average molar mass of the sample M_w, which can be related

142 to the intensity of scattered light using equation (3), where c is the polymer concentration,

143 K^* an instrumental constant, R_G the radius of gyration of the polymer particles, λ the

144 wavelength of incident light and A_2 the second virial coefficient of the polymer solution. R_θ is

145 the excess Rayleigh ratio, which is directly proportional to the intensity of scattered light at

146 the angle θ. This equation shows that for a given polymer concentration, cK^*/R_θ is linearly

147 dependent from $\sin^2\theta/2$. The intercept of this line equals the second bracket in the equation,

148 which can be used to calculate M_w if A_2 and c are known.

149

150 $$(3)\ \frac{cK^*}{R_\theta} = \left(1 + \frac{16\pi^2 R_G^2}{3\lambda^2}\sin^2\theta/2\right)\left(\frac{1}{M_w} + 2A_2 c\right)$$

151

152 Once M_w is obtained, the degree of polymerization can be calculated from M_w dividing by the

153 molar mass of a monomer. The yield of the carbanilation of cellulose is known to be 97.5%

154 (Daňhelka et al., 1976), and therefore the molar mass of the monomer is approximately 510.5

155 g mol^{-1}.

156

157 **2.5 EGA-MS:** Evolved gas analyses were carried out with an EGA/Py-3030D micro-furnace

158 pyrolyzer (Frontier Lab, Japan) coupled to a 6890 gas chromatograph (Agilent Technologies,

159 USA) equipped with a deactivated and uncoated stainless steel column (UADTM-2.5N, 2.5 m

160 x 0.15 mm, Frontier Lab, Japan). 50 µg of sample were used for each EGA. In all experiments,

161 the temperature of the pyrolysis furnace was raised from 100 to 600 °C. Heating rates of 5,

162 10 and 20 °C min^{-1} were used for all samples. Helium (1 mL min^{-1}) was used as carrier gas.

Injection was performed in split mode with a split ratio of 100:1. The GC oven and injector were kept at 300 °C during all analyses. Detection was carried out with a 5973 Mass Selective detector (Agilent Technologies, USA), operating in EI positive mode (70 eV, mass range m/z 50-300). The thermograms were processed using MSD ChemStation (Agilent Technologies, USA). Experiments were repeated three times to assess the reproducibility of the thermograms. Relative standard deviations were lower than 10%.

The thermograms were used to obtain apparent activation energy values using model-free isoconversional methods. For this purpose, conversion profiles were calculated from the thermograms using $\alpha(T) = I(T)/I_{tot}$, where α is the conversion, $I(T)$ the cumulative integral of the thermogram up to the temperature T, and I_{tot} is the total integral of the thermogram. Two different isoconversional data processing methods were used: the Kissinger-Akahira-Sunose method (KAS) and the Flynn-Wall-Ozawa method (FWO). The equations for these methods are (4) and (5), where β is the heating rate, T the temperature, E_a the apparent activation energy, R the gas constant, and $q(\alpha)$ and $r(\alpha)$ are functions of the conversion. For a fixed value of α, these equations give a linear trend of the left side with respect to 1/T, and the slope can be directly related to the apparent activation energy of the thermal degradation process.

$$(1)\ \ln\frac{\beta}{T^2} = -\frac{E_a}{RT} + q(\alpha)$$

$$(2)\ \ln\beta = -1.052\frac{E_a}{RT} + r(\alpha)$$

3. RESULTS AND DISCUSSION

3.1 ATR-FTIR: ~~The ATR-FTIR spectra obtained for Sigmacell 20 cellulose at all milling times are reported in Figure 1a, and peak attributions are reported in Table 1.~~ ATR-FTIR spectra obtained for Sigmacell 20 cellulose at all milling times and peak attributions are reported in Figure S1a and Table S1 in Supplementary Materials, respectively. When milling time was increased, a significant loss in resolution for some of the absorption bands was observed. This alteration of the spectra was attributed to a reduction in the cellulose crystallinity. While the orderly structure of crystalline cellulose generates sharp and resolved peaks, amorphous cellulose generates broad peaks, most likely due to broader distributions of the transition energies (Široký et al., 2010). In addition, ATR is sensitive to crystal size: upon the decrease in crystal size more light scattering is observed which is manifested by the increase of the base line absorption. The changes after ball-milling were particularly evident for the bands at 1051, 1103, 1317, 1335, 1362 and 1418 cm^{-1}. Similar changes were reported by Schwanninger and co-workers in FTIR transmittance analyses of spruce wood after short-time ball milling (Schwanninger et al., 2004).

Other changes in the spectral profile were observed for bands at 1027-1019 and 1159-1155 cm^{-1} (#3 and 6 in ~~Figure 1a and Table 1~~ Figure S1a and Table S1), which can be attributed to C-O-C vibrations. While the bands intensities remained unaltered, the wavenumber of maximum absorption shifted to smaller values as the milling time was increased. It is likely that the cleavage of hydrogen bonds due to ball-milling allowed these bonds to change their equilibrium distances and conformations, resulting in different vibrational energies. The shift in absorption maxima was also reported by Schwanninger and co-workers for most of the cellulose signals (Schwanninger et al., 2004).

207

Crystallinity of all samples was estimated from the ATR-FTIR spectra by calculating the ratio

of peaks at 1426 and 895 cm^{-1} (Nelson & O'Connor, 1964). The results are reported in Figure

1~~c~~a and ~~Table 2~~ Table 1. The CI derived from FTIR cannot be treated as absolute measure of

crystallinity, but it can be used for comparative assessment of the samples. All samples

showed a decreasing trend in the obtained CI values upon milling time. The most profound

changes were noted for the initial period of milling (30 min). This is in accordance with the

band broadening, which is more evident after 30 minutes of milling.

215

3.2 XRD: The XRD spectra obtained for Sigmacell 20 cellulose are reported in ~~Figure 1b~~ Figure

S1b in the Supplementary Materials. The diffraction pattern corresponds to cellulose I$_\beta$ phase,

with diffraction peaks at 2θ = 14.5°, 16.2°, 20.5°, 22.4° and 33.9°, corresponding to the (101),

(10-1), (201), (002) and (040) diffraction planes, respectively. Cellulose Iβ ~~which~~ is the most

common cellulose allomorph in nature (French, 2014; French & Santiago Cintrón, 2013). As

expected, the intensity of the reflection signals decreased upon milling time. Similarly to the

ATR-FTIR results, the smoothing of the diffractograms was most evident in the first 30 min of

milling, and less evident for the other milling times. The intensity reduction of the peaks is

also manifested by the decrease in the signal-to-noise ratio going from 60 to 120 min milled

samples. After 2 hours of milling, the diffractograms were dominated by the signal of the

amorphous phase, which is centred at approximately 2θ = 19°.

The diffractograms were processed by peak fitting, using five Gaussian functions

corresponding to each of the ~~four~~ five reflection functions of crystalline cellulose, and a sixth

Gaussian function for the amorphous phase (Park et al., 2010). The resulting CI values are

230 reported in ~~Table 2~~ Table 1, while a graph showing the CI trends for all samples is reported in

231 Figure 1d. The initial CIs were higher than 0.6 for Sigmacell 50 and Sigmacell 20, and higher

232 than 0.7 for microcrystalline and acid-washed celluloses. ~~After 120 minutes of milling, the CI~~

233 ~~values decreased by 20% on average.~~ Similarly to the FTIR results, the most significant drop

234 in CI was observed for all samples after 30 minutes of milling, while all subsequent milling

235 times had less profound effects. After 120 minutes of milling, the CI values decreased by 80%

236 on average. Comparing cellulose samples from different sources, the greatest decrease in CI

237 was observed for microcrystalline cellulose (~~22%~~ 93%), while the smallest - for Sigmacell 20

238 Sigmacell 50 and acid-washed cellulose (~~16%~~ 73%). There is a high positive correlation (r =

239 0.94) between the percentage decrease in CI and the starting CI value for all samples. This

240 suggests that ball milling tends to reduce the crystallinity of cellulose up to an asymptotic

241 value, which means that the samples with higher starting CIs will be more affected. We have

242 found also a good correlation between the CI values obtained from ATR-FTIR and from XRD (r

243 = 0.97), which indicates that both methods can be used to monitor the loss of crystallinity.

244 The dimensions of the crystalline domains obtained by using the Scherrer equation for the

245 un-milled samples are reported in ~~Table 2~~ Table 1. The diffraction peak at 2θ = 22.4° was used

246 in all four cases for the calculation. Estimation of the crystallite dimensions for all milled

247 samples was difficult and unreliable due to the loss in peak intensity. Acid-washed cellulose

248 showed the greatest crystallite dimension, while Sigmacell 50 cellulose showed the smallest.

249 There is no apparent correlation between the crystallite dimensions and the CI decrease after

250 two hours of milling, suggesting that the efficiency of ball-milling does not depend on τ.

251

3.3 SEC-UV- MALS-DRI: Figure 2a shows the molar mass distribution for Sigmacell 20 at all

milling times. The DP values derived from the SEC results for all samples are reported in ~~Table~~

~~2~~ Table 1, and a graphic representation is given in Figure 2b. All un-milled cellulose samples

showed similar degrees of polymerization, although the plant source is not the same for every

sample. This could be due to similar extraction or purification processes. Acid-washed

cellulose showed the highest DP which amounts to 283, while microcrystalline cellulose

showed the lowest DP - 232. Both Sigmacell celluloses had initial DPs values of 251.

After milling, both a slight shift of the peak maxima and a peak broadening in the molecular

mass distribution curves were observed (Figure 2a). These results are consistent with the

decrease in degree of polymerisation. The extent of this decrease was different for all

samples: acid-washed cellulose was the most affected, and after two hours its DP dropped to

192; Sigmacell 20 was the least affected, reaching 218 after two hours of milling;

microcrystalline cellulose remained the least polymerized at all milling times, dropping from

114 to 102 (10%).

Coefficients of variations (CVs) on the DP values were generally lower than 3%, with few

exceptions. If the un-milled and 120 minutes milled samples are compared using Student's t-

test, the variations in DP prove to be statistically significant for all cellulose samples at a 95%

confidence. Although the effect of ball-milling on the DP is usually overlooked, these results

show that it should be considered during pre-treatment of cellulose samples. Finally, it is

interesting to note that the trends in DP and CI with milling time are different. While the

decrease in CI is more drastic in the first 30 minutes of milling, the decrease in DP is more

homogeneous along the whole investigated time range. This is also shown by the average

274 correlation coefficients between milling time and CI (r = –0.88) and between milling time and

275 DP (r = –0.98).

276

277 **3.4 EGA-MS:** The set of thermograms obtained from EGA-MS for un-milled Sigmacell 20

278 cellulose is reported ~~at the top of Figure 3~~ in Figure 3a. As the heating rate was increased, the

279 gas evolution peak moved to higher temperatures. The thermograms were processed with

280 model-free isoconversional methods, to obtain apparent activation energy values for

281 cellulose pyrolysis. ~~To use isoconversional methods, conversion profiles were calculated from~~

282 ~~the thermograms using α(T) = I(T)/I~tot~, where α is the conversion, I(T) the cumulative integral~~

283 ~~of the thermogram up to the temperature T, and I~tot~ is the total integral of the thermogram.~~

284 ~~Two different isoconversional data processing methods were used: the Kissinger-Akahira-~~

285 ~~Sunose method (KAS) and the Flynn-Wall-Ozawa method (FWO). The equations for these~~

286 ~~methods are (4) and (5), where β is the heating rate, T the temperature, E~a~ the apparent~~

287 ~~activation energy, R the gas constant, and q(α) and r(α) are functions of the conversion. For a~~

288 ~~fixed value of α, these equations give a linear trend of the left side with respect to 1/T, and~~

289 ~~the slope can be directly related to the apparent activation energy of the thermal degradation~~

290 ~~process.~~

291

292 ~~(3) $\ln \frac{\beta}{T^2} = -\frac{E_\alpha}{RT} + q(\alpha)$~~

293 ~~(4) $\ln \beta = -1.052 \frac{E_\alpha}{RT} + r(\alpha)$~~

294

295 For each sample, seven different conversion values were chosen to perform linear regression,

296 ranging from α = 0.2 to α = 0.8. The seven slopes were averaged to obtain an estimation of

297 E_a. The results are reported in ~~Table 3~~ Table 1, and ~~a graphical representation~~ graphical

298 representations of the trends ~~is~~ are shown in ~~the bottom row of Figure 3~~ Figure 3e and f.

299 Sigmacell 50 cellulose showed the highest E_a at all milling times, with a starting value of 136-

300 139 kJ/mol. On the other hand, microcrystalline cellulose showed the lowest starting E_a with

301 114-118 kJ/mol. After 120 minutes of milling, the E_a decreased by about 10% on average.

302 Sigmacell 50 cellulose showed the greatest drop (16-17%), while microcrystalline cellulose

303 showed the smallest (9-10%). The E_a values for the un-milled samples are similar to those

304 found by previous studies using isoconversional methods (Ali et al., 2017; Dahiya et al., 2008;

305 Kim et al., 2017; Sánchez-Jiménez et al., 2011). However, it should be pointed out that the

306 activation energy values obtained by isoconversional methods are only an approximation of

307 the intrinsic activation energy involved in the whole pyrolysis process. This is because the

308 intrinsic activation energy can be derived only if the pyrolysis mechanism is known or at least

309 the kinetic equation is derived. Therefore, the values of E_a obtained in this work should only

310 be used for comparison of samples treated under the same conditions.

311 CVs on the E_a values were lower by 5% in most of the cases, with few exceptions. The

312 differences between E_a values were evaluated with Student's and Welch's tests at a 95%

313 confidence. The differences between the un-milled and the 120 minutes milled samples

314 proved to be statistically relevant in all four cases. Moreover, all the E_a variations with milling

315 time were statistically relevant for both Sigmacell 50 and Sigmacell 20 cellulose. An

316 anomalous trend was observed for acid-washed cellulose, for which the E_a value after two

317 hours of milling was greater than the one after one hour. However, the differences among E_a

values of acid-washed cellulose at 30, 60 and 120 minutes of milling proved to be statistically

negligible (Student's t-test, 95% confidence).

The two isoconversional methods provided E_a values with good correlation (r = 0.99). However, it is evident by looking at the values themselves that the FWO method provides higher values than the KAS method. The 2003 paper by Starink (Starink, 2003) can be used to estimate the error of the two isoconversional methods depending on the value of E_a/RT. In this case, the error associated with FWO method is approximately one order of magnitude bigger than the error associated with the KAS method (3% and 0.3%, respectively).

To obtain additional insight into the effect of milling on the cellulose strands, average mass spectra were obtained from the EGA thermograms. The average mass spectra of un-milled and 2-hours milled Sigmacell 20 are shown in Figure S2 in the Supplementary Materials. Similar results were obtained for all other cellulose samples. As can be noted, the two spectra showed the same profiles. The main signals at m/z 60 and 73 can be attributed to fragment ions of levoglucosan, which is the main pyrolysis product of cellulose (Tamburini et al., 2015). This result suggests that, although ball-milling reduced the apparent activation energy of cellulose pyrolysis, it had no effect on the chemical structure of the cellulose strands, and therefore the pyrolysis mechanism of the samples was not altered. This means that the decrease in apparent activation energy is due to the decrease of CI and DP.

A recent publication by Sanchez-Jimenez and co-workers (Sánchez-Jiménez et al., 2011) used model-based isoconversional methods and observed that random-chain scission is the most suitable model to represent the pyrolysis mechanism of cellulose. This result is very important, as it suggests that the degree of polymerisation has little impact on the energy required for the pyrolysis of cellulose. This brings us to the conclusion that the main cause for

the decrease in apparent activation energy for the pyrolysis of cellulose is the decrease in

crystallinity. This is consistent with the fact that isoconversional methods provide an energy

value that considers all transformations taking place in the sample during pyrolysis, and

therefore the apparent activation energy values must include the energy required to cleave

the crystalline lattice.

Following this hypothesis, the apparent activation energies obtained with the KAS method,

which proved to be the most accurate, were plotted against the CIs obtained from the XRD

measurements, and linear regression was performed on the four cellulose samples separately

using equation (6).

(5) $E_a = E_1 + E_2 \cdot CI$

Equation (6) shows that a hypothetical fully-crystalline cellulose sample (CI = 1) would have

an apparent activation energy equal to E_1 + E_2, while a fully-amorphous sample (CI = 0) would

have an apparent activation energy equal to E_1. The value of E_2 is therefore an estimation of

the apparent activation energy for the cleavage of the crystalline lattice of cellulose.

The results are reported in Figure 4 and Table 2. Good R^2 values were obtained for all

cellulose samples. The slopes of the regression curves ranged from 18.1 kJ/mol for

Microcrystalline cellulose to 44.8 kJ/mol for Sigmacell 50. Averaging of the four slopes gave

30 kJ/mol. On the other hand, the four intercepts showed much smaller variation, and

averaging of the four intercepts gave 102 kJ/mol.

The lower error on the average intercept suggests that the apparent activation energy of the

pyrolysis process has been estimated with more accuracy than the apparent activation energy

for the amorphization process. A likely reason for this result is that there are some additional

17

365 contributions to the energy of the crystalline lattice, which are different among the various

366 samples and are not considered in the proposed model. A possible additional factor could be

367 a different spatial arrangement of the crystallites inside the amorphous phase, or a

368 heterogeneous distribution of the two phases in the cellulose powder.

369

370 **4. CONCLUSIONS**

371 Ball-milling of cellulose gave rise to an average decrease of 80% in crystallinity indices

372 derived from FTIR and XRD analyses. The crystallinity drop showed an asymptotic trend.

373 The DP decreased by 20% on average, with approximately linear trend. This is an important

374 observation since the effect of ball-milling on the DP is usually neglected.

375 Apparent activation energy values decreased by 10% on average, indicating that

376 depolymerization and amorphization significantly reduce thermal stability.

377 We believe that the results provided here will contribute to the discussion on the effects of

378 ball-milling on cellulose, and could be used to optimize cellulose conversion processes.

379

388   **REFERENCES**

389   [1] Agarwal, U.P., Reiner, R.S., Ralph, S.A. 2010. Cellulose I crystallinity determination using FT–Raman
390   spectroscopy: univariate and multivariate methods. *Cellulose*, **17**(4), 721-733.
391   [2] Ali, I., Bahaitham, H., Naebulharam, R. 2017. A comprehensive kinetics study of coconut shell waste
392   pyrolysis. *Bioresource Technology*, **235**, 1-11.
393   [3] Alvira, P., Tomás-Pejó, E., Ballesteros, M., Negro, M. 2010. Pretreatment technologies for an
394   efficient bioethanol production process based on enzymatic hydrolysis: a review. *Bioresource*
395   *Technology*, **101**(13), 4851-4861.
396   [4] Avolio, R., Bonadies, I., Capitani, D., Errico, M., Gentile, G., Avella, M. 2012. A multitechnique
397   approach to assess the effect of ball milling on cellulose. *Carbohydrate Polymers*, **87**(1), 265-
398   273.
399   [5] Bledzki, A.K., Gassan, J. 1999. Composites reinforced with cellulose based fibres. *Progress in*
400   *Polymer Science*, **24**(2), 221-274.
401   [6] da Silva, A.S.A., Inoue, H., Endo, T., Yano, S., Bon, E.P.S. 2010. Milling pretreatment of sugarcane
402   bagasse and straw for enzymatic hydrolysis and ethanol fermentation. *Bioresource*
403   *Technology*, **101**(19), 7402-7409.
404   [7] Dahiya, J.B., Kumar, K., Muller-Hagedorn, M., Bockhorn, H. 2008. Kinetics of isothermal and non-
405   isothermal degradation of cellulose: model-based and model-free methods. *Polymer*
406   *International*, **57**(5), 722-729.
407   [8] Daňhelka, J., Kössler, I., Boháčková, V. 1976. Determination of molecular weight distribution of
408   cellulose by conversion into tricarbanilate and fractionation. *Journal of Polymer Science Part*
409   *A: Polymer Chemistry*, **14**(2), 287-298.
410   [9] De Silva, R., Byrne, N. 2017. Utilization of cotton waste for regenerated cellulose fibres: influence
411   of degree of polymerization on mechanical properties. *Carbohydrate Polymers*.
412   [10] French, A.D. 2014. Idealized powder diffraction patterns for cellulose polymorphs. *Cellulose*,
413   **21**(2), 885-896.
414   [11] French, A.D., Santiago Cintrón, M. 2013. Cellulose polymorphy, crystallite size, and the Segal
415   Crystallinity Index. *Cellulose*, **20**(1), 583-588.
416   [12] Gu, B.-J., Wang, J., Wolcott, M.P., Ganjyal, G.M. 2018. Increased sugar yield from pre-milled
417   Douglas-fir forest residuals with lower energy consumption by using planetary ball milling.
418   *Bioresource Technology*, **251**, 93-98.
419   [13] Hallac, B.B., Ragauskas, A.J. 2011. Analyzing cellulose degree of polymerization and its relevancy
420   to cellulosic ethanol. *Biofuels, Bioproducts and Biorefining*, **5**(2), 215-225.
421   [14] Kaur, R., Gera, P., Jha, M.K., Bhaskar, T. 2018. Pyrolysis kinetics and thermodynamic parameters
422   of castor (Ricinus communis) residue using thermogravimetric analysis. *Bioresource*
423   *Technology*, **250**, 422-428.
424   [15] Kian, L.K., Jawaid, M., Ariffin, H., Karim, Z. 2018. Isolation and characterization of nanocrystalline
425   cellulose from roselle-derived microcrystalline cellulose. *International Journal of Biological*
426   *Macromolecules*.
427   [16] Kim, Y.-M., Han, T.U., Hwang, B., Lee, Y., Watanabe, A., Teramae, N., Kim, S.-S., Park, Y.-K., Kim, S.
428   2017. New approach for the kinetic analysis of cellulose using EGA-MS. *Polymer Testing*, **60**,
429   12-17.
430   [17] Lavoine, N., Desloges, I., Dufresne, A., Bras, J. 2012. Microfibrillated cellulose–Its barrier
431   properties and applications in cellulosic materials: A review. *Carbohydrate Polymers*, **90**(2),
432   735-764.
433   [18] Lee, H., Mani, S. 2017. Mechanical pretreatment of cellulose pulp to produce cellulose nanofibrils
434   using a dry grinding method. *Industrial Crops and Products*, **104**(Supplement C), 179-187.
435   [19] Łojewska, J., Miśkowiec, P., Łojewski, T., Proniewicz, L. 2005. Cellulose oxidative and hydrolytic
436   degradation: In situ FTIR approach. *Polymer Degradation and Stability*, **88**(3), 512-520.

437 [20] Łojewski, T., Zięba, K., Łojewska, J. 2010. Size exclusion chromatography and viscometry in paper
438   degradation studies. New Mark-Houwink coefficients for cellulose in cupri-ethylenediamine.
439   *Journal of Chromatography A*, **1217**(42), 6462-6468.
440 [21] Marx-Figini, M., Maximino, M. 1993. Effect of impregnation on the degree of polymerization of
441   cellulose during bleaching of sodapulped sugar cane bagasse. *Macromolecular Materials and*
442   *Engineering*, **208**(1), 167-172.
443 [22] Mukarakate, C., Mittal, A., Ciesielski, P.N., Budhi, S., Thompson, L., Iisa, K., Nimlos, M.R., Donohoe,
444   B.S. 2016. Influence of crystal allomorph and crystallinity on the products and behavior of
445   cellulose during fast pyrolysis. *ACS Sustainable Chemistry & Engineering*, **4**(9), 4662-4674.
446 [23] Nelson, M.L., O'Connor, R.T. 1964. Relation of certain infrared bands to cellulose crystallinity and
447   crystal latticed type. Part I. Spectra of lattice types I, II, III and of amorphous cellulose. *Journal*
448   *of Applied Polymer Science*, **8**(3), 1311-1324.
449 [24] Ni, J., Teng, N., Chen, H., Wang, J., Zhu, J., Na, H. 2015. Hydrolysis behavior of regenerated
450   celluloses with different degree of polymerization under microwave radiation. *Bioresource*
451   *Technology*, **191**, 229-233.
452 [25] Ogundare, S.A., Moodley, V., van Zyl, W.E. 2017. Nanocrystalline cellulose isolated from discarded
453   cigarette filters. *Carbohydrate Polymers*, **175**, 273-281.
454 [26] Park, S., Baker, J., Himmel, M., Parilla, P., Johnson, D. 2010. Cellulose crystallinity index:
455   measurement techniques and their impact on interpreting cellulase performance.
456   *Biotechnology for Biofuels*, **3**(1), 1-10.
457 [27] Pawcenis, D., Thomas, J.L., Łojewski, T., Milczarek, J.M., Łojewska, J. 2015. Towards determination
458   of absolute molar mass of cellulose polymer by size exclusion chromatography with mulitple
459   angle laser light scattering detection. *Journal of Chromatography A*, **1409**, 53-59.
460 [28] Podzimek, S. 2011. *Light scattering, size exclusion chromatography and asymmetric flow field flow*
461   *fractionation: powerful tools for the characterization of polymers, proteins and nanoparticles*.
462   John Wiley & Sons.
463 [29] Podzimek, S. 2014. Truths and myths about the determination of molar mass distribution of
464   synthetic and natural polymers by size exclusion chromatography. *Journal of Applied Polymer*
465   *Science*, **131**(7).
466 [30] Qiu, X., Hu, S. 2013. "Smart" materials based on cellulose: a review of the preparations,
467   properties, and applications. *Materials*, **6**(3), 738-781.
468 [31] Rebière, J., Heuls, M., Castignolles, P., Gaborieau, M., Rouilly, A., Violleau, F., Durrieu, V. 2016.
469   Structural modifications of cellulose samples after dissolution into various solvent systems.
470   *Analytical and Bioanalytical Chemistry*, **408**(29), 8403-8414.
471 [32] Sánchez-Jiménez, P.E., Pérez-Maqueda, L.A., Perejón, A., Pascual-Cosp, J., Benítez-Guerrero, M.,
472   Criado, J.M. 2011. An improved model for the kinetic description of the thermal degradation
473   of cellulose. *Cellulose*, **18**(6), 1487-1498.
474 [33] Schenzel, K., Fischer, S., Brendler, E. 2005. New method for determining the degree of cellulose I
475   crystallinity by means of FT Raman spectroscopy. *Cellulose*, **12**(3), 223-231.
476 [34] Schwanninger, M., Rodrigues, J., Pereira, H., Hinterstoisser, B. 2004. Effects of short-time
477   vibratory ball milling on the shape of FT-IR spectra of wood and cellulose. *Vibrational*
478   *Spectroscopy*, **36**(1), 23-40.
479 [35] Siqueira, G., Bras, J., Dufresne, A. 2010. Cellulosic bionanocomposites: a review of preparation,
480   properties and applications. *Polymers*, **2**(4), 728-765.
481 [36] Široký, J., Blackburn, R.S., Bechtold, T., Taylor, J., White, P. 2010. Attenuated total reflectance
482   Fourier-transform Infrared spectroscopy analysis of crystallinity changes in lyocell following
483   continuous treatment with sodium hydroxide. *Cellulose*, **17**(1), 103-115.
484 [37] Starink, M. 2003. The determination of activation energy from linear heating rate experiments: a
485   comparison of the accuracy of isoconversion methods. *Thermochimica Acta*, **404**(1), 163-176.

486   [38] Tamburini, D., Łucejko, J.J., Ribechini, E., Colombini, M.P. 2015. Snapshots of lignin oxidation and
487   depolymerization in archaeological wood: an EGA-MS study. *Journal of Mass Spectrometry*,
488   **50**(10), 1103-1113.
489   [39] Wang, S., Dai, G., Yang, H., Luo, Z. 2017. Lignocellulosic biomass pyrolysis mechanism: A state-of-
490   the-art review. *Progress in Energy and Combustion Science*, **62**, 33-86.
491   [40] Xu, F., Yu, J., Tesso, T., Dowell, F., Wang, D. 2013. Qualitative and quantitative analysis of
492   lignocellulosic biomass using infrared techniques: a mini-review. *Applied Energy*, **104**, 801-
493   809.
494   [41] Yang, C.-H., Chen, C.-A., Chen, C.-F. 2018. Surface-Modified Cellulose Paper and Its Application in
495   Infectious Disease Diagnosis. *Sensors and Actuators B: Chemical*.
496   [42] Yue, Y., Han, J., Han, G., Zhang, Q., French, A.D., Wu, Q. 2015. Characterization of cellulose I/II
497   hybrid fibers isolated from energycane bagasse during the delignification process:
498   Morphology, crystallinity and percentage estimation. *Carbohydrate Polymers*, **133**, 438-447.
499   [43] Zhao, D., Yang, F., Dai, Y., Tao, F., Shen, Y., Duan, W., Zhou, X., Ma, H., Tang, L., Li, J. 2017. Exploring
500   crystalline structural variations of cellulose during pulp beating of tobacco stems.
501   *Carbohydrate Polymers*, **174**(Supplement C), 146-153.

502

503

504

505 **Figure 1:** ~~(a) ATR-FTIR spectra of Sigmacell 20 cellulose at different milling times. The signals~~

506 ~~are normalised by the correction factor. Peaks are numbered according to Table 1; (b) XRD~~

507 ~~spectra of Sigmacell type 20 at different milling times. The peaks are labelled using Miller~~

508 ~~indices; (c)~~ CI trends obtained by (a) ATR-FTIR and ~~(d)~~ (b) XRD spectra for all cellulose samples

509 at all milling times. S20 = Sigmacell 20; S50 = Sigmacell 50; SMC = Microcrystalline cellulose;

510 SAW = acid-washed cellulose.

511

512 **Figure 2:** (a) molar mass distribution plots for Sigmacell 20 at all milling times; (b) degrees of

513 polymerization for all samples at all milling times. S20 = Sigmacell 20; S50 = Sigmacell 50; SMC

514 = Microcrystalline cellulose; SAW = acid-washed cellulose.

515

516 **Figure 3:** (a) normalized thermograms obtained by EGA-MS for un-milled Sigmacell 20

517 cellulose at different heating rates; (b) conversion profiles obtained by integration of the

518 thermograms in (a); (c) linear regression curves obtained using the KAS and (d) FWO methods

519 for un-milled Sigmacell 20 cellulose at conversion values from 0.2 to 0.8; (e) trends in E_a values

520 obtained using the KAS and (f) FWO methods. S20 = Sigmacell 20; S50 = Sigmacell 50; SMC =

521 Microcrystalline cellulose; SAW = acid-washed cellulose.

522

523 **Figure 4:** Plots of E_a values obtained with the KAS method and CI values from XRD for all

524 cellulose samples.

525

Table 1: Crystallinity indices obtained by FTIR and XRD, crystallite dimensions, degrees of polymerization obtained by SEC and apparent activation energies obtained by EGA-MS using KAS and FWO isoconversional methods for all samples.

Sample	Milling time (min)	CI by FTIR	CI by XRD	τ (nm)	DP by SEC	E_a by KAS (kJ/mol)	E_a by FWO (kJ/mol)
Sigmacell 20	0	1.05	0.63	6.43	251 ± 5	122 ± 2	126 ± 2
	30	0.67	0.37		249 ± 6	113 ± 2	117 ± 2
	60	0.55	0.26		232 ± 3	110 ± 2	114 ± 1
	120	0.52	0.15		218 ± 1	106 ± 2	111 ± 2
Sigmacell 50	0	0.90	0.67	5.29	250 ± 10	136 ± 8	139 ± 7
	30	0.59	0.33		235 ± 1	126 ± 3	129 ± 3
	60	0.61	0.28		233 ± 3	119 ± 2	123 ± 2
	120	0.60	0.18		206 ± 6	113 ± 1	117 ± 1
Microcrystalline	0	0.87	0.73	6.00	232 ± 6	114 ± 9	118 ± 8
	30	0.56	0.37		227 ± 1	110 ± 2	114 ± 2
	60	0.46	0.17		213 ± 2	104 ± 4	108 ± 4
	120	0.46	0.05		183 ± 1	102 ± 6	106 ± 5
Acid-washed	0	0.87	0.75	8.18	283 ± 8	122 ± 8	125 ± 7
	30	0.72	0.33		266 ± 3	108 ± 4	113 ± 4
	60	0.66	0.25		250 ± 20	105 ± 3	110 ± 3
	120	0.63	0.20		192 ± 7	108 ± 1	112 ± 1

531   *Table 2:* Intercept, slope and R^2 values for the plots of apparent activation energy against CI

532   of all cellulose samples. Average intercept and slope are also reported.

Sample	INT ($\cdot 10^5$ J/mol)	SLO ($\cdot 10^4$ J/mol)	R^2
Sigmacell 20	1.01	3.30	0.98
Sigmacell 50	1.07	4.48	0.88
Microcrystalline	1.01	1.81	0.92
Acid-washed	1.00	2.86	0.91
Average	1.02 ± 0.02	3.00 ± 1.00	

533

534

535

536

537

538

541

542

543
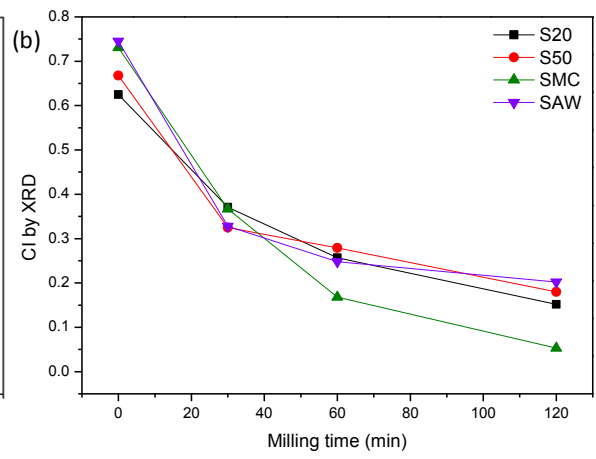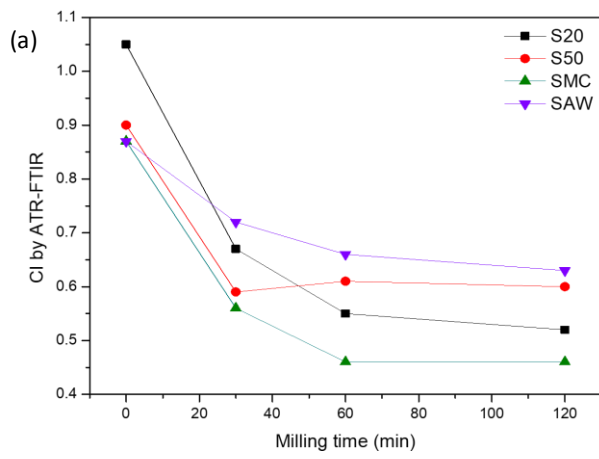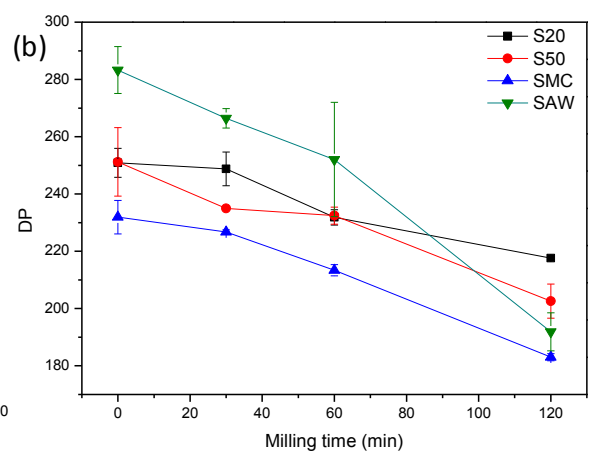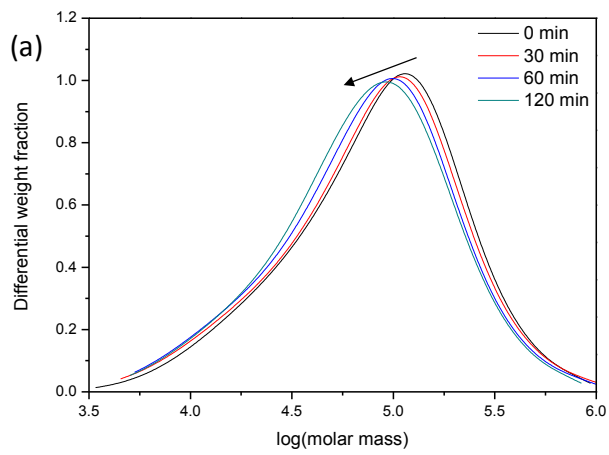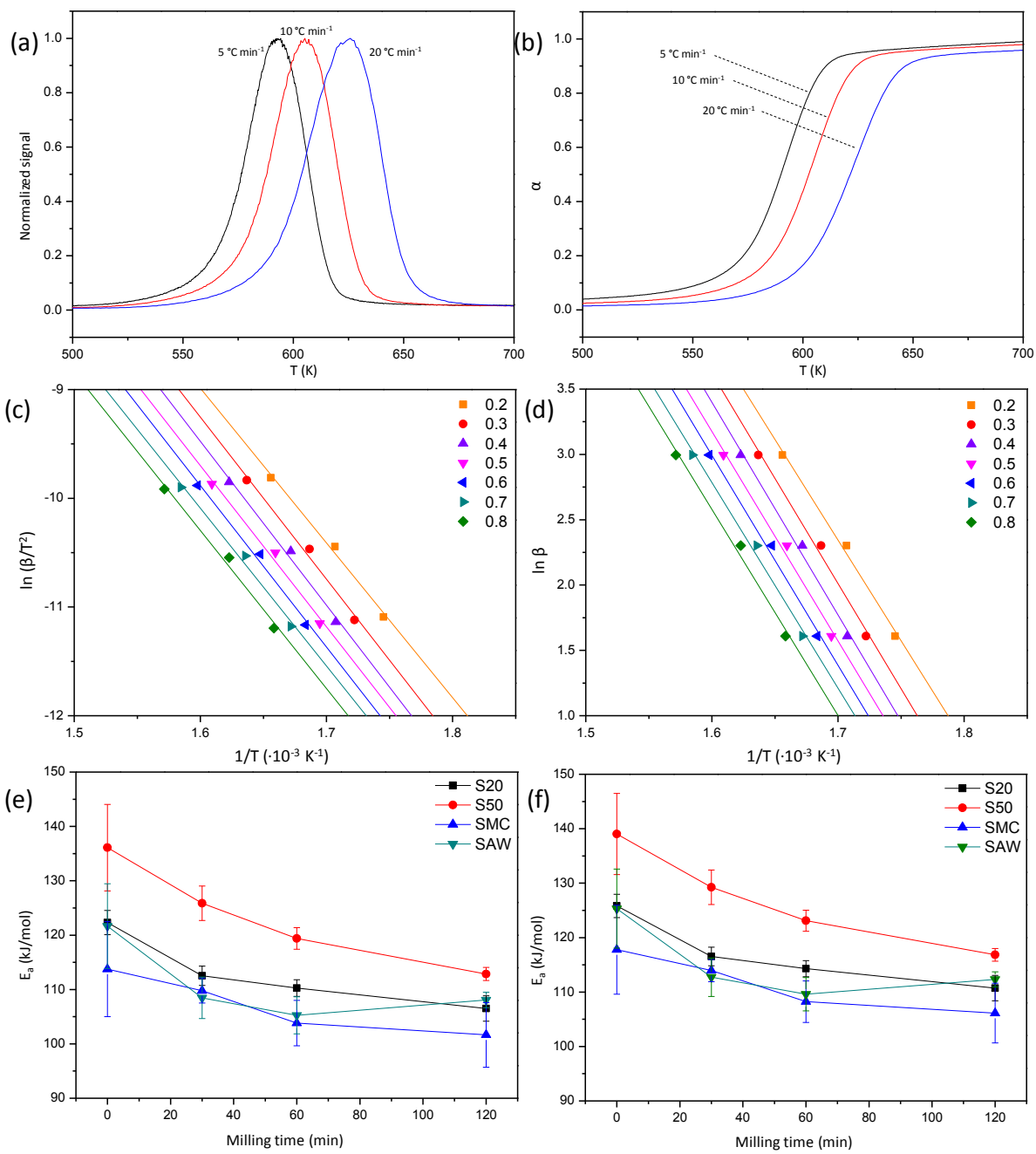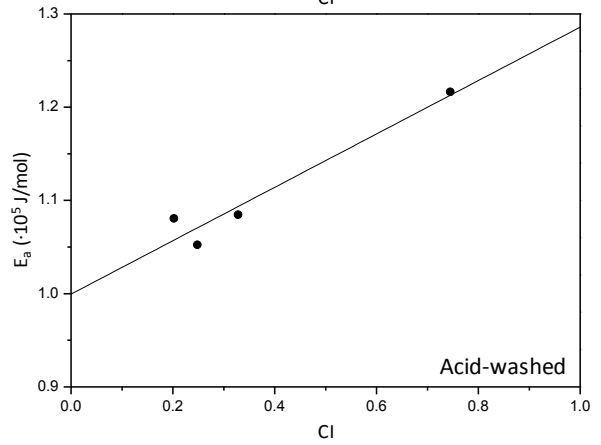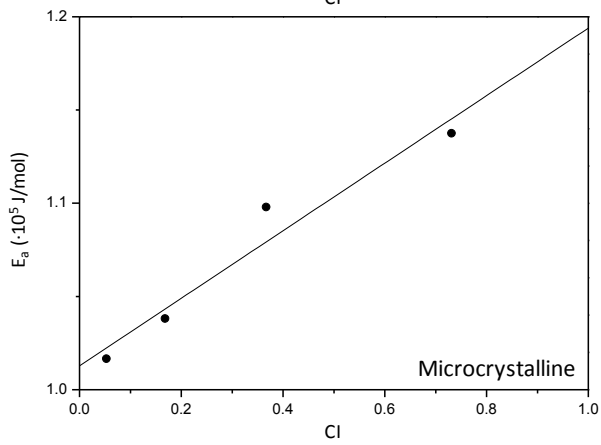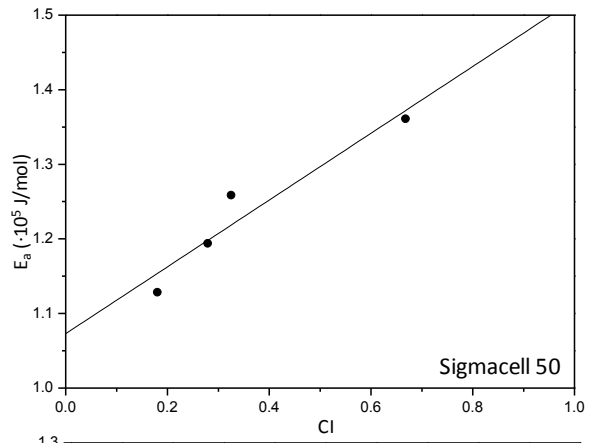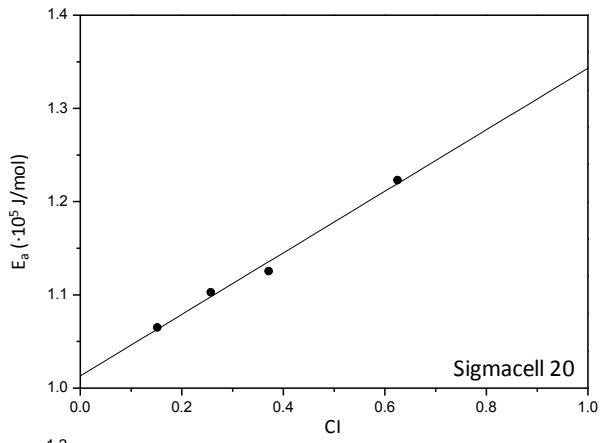
545   *Table S1:* Peak attributions for the ATR-FTIR spectra.

| Peak #	cm^{-1}	Attribution	Reference
1	894	C-O-C, C-C-O, C-C-H stretching	(Schwanninger et al., 2004; Xu et al., 2013; Zhao et al., 2017)
2	985	C-O valence vibration	(Schwanninger et al., 2004; Xu et al., 2013)
3	1027-1019	C-O-C asymmetric stretching	(Ogundare et al., 2017)
4	1051	C-O valence vibration	(Zhao et al., 2017)
5	1103	Ring asymmetric valence vibration	(Zhao et al., 2017)
6	1159-1155	C-O-C asymmetric valence vibration	(Schwanninger et al., 2004; Xu et al., 2013; Zhao et al., 2017)
7	1199	O-H bending	(Schwanninger et al., 2004; Xu et al., 2013)
8	1281	C-H bending	(Schwanninger et al., 2004; Xu et al., 2013)
9	1317	CH$_2$ wagging	(Schwanninger et al., 2004; Xu et al., 2013)
10	1335	C-H vibration, O-H bending	(Schwanninger et al., 2004; Xu et al., 2013; Zhao et al., 2017)
11	1362	C-H asymmetric bending	(Ogundare et al., 2017)
12	1418	H-C-H, O-C-H scissoring	(Schwanninger et al., 2004; Zhao et al., 2017)

546

547
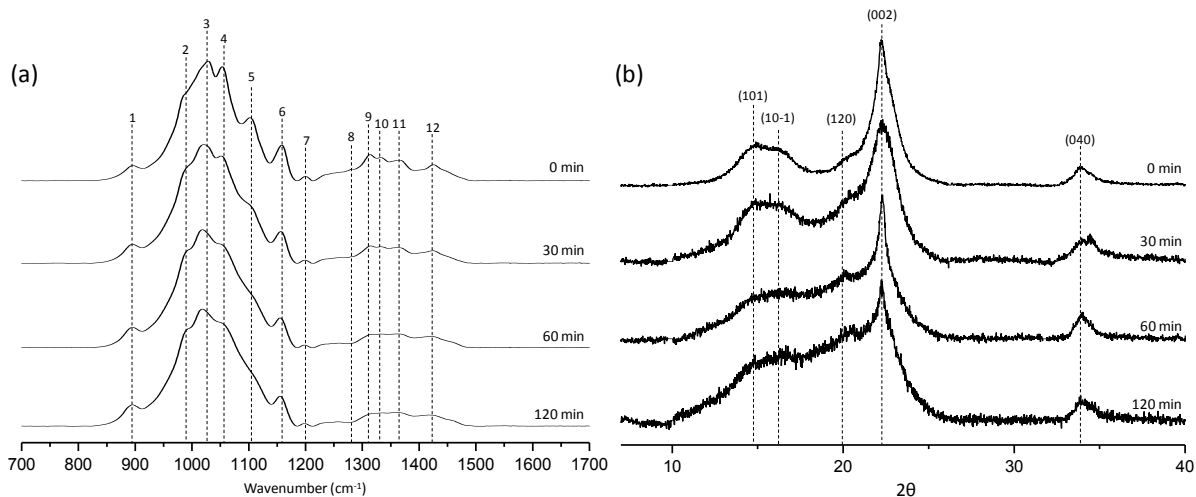
548

549   ***Figure S1:*** (a) ATR-FTIR spectra of Sigmacell 20 cellulose at different milling times. The

550   signals are normalised by the correction factor. Peaks are numbered according to Table 1;

551   (b) XRD spectra of Sigmacell type 20 at different milling times. The peaks are labelled using

552   Miller indices.

553
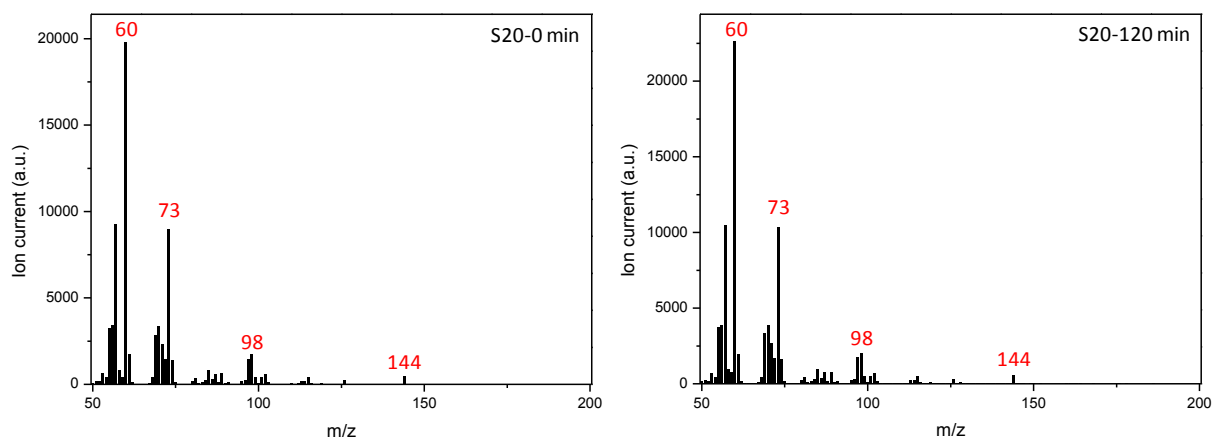
554

555 ***Figure S2:*** Average mass spectra from EGA-MS profiles of un-milled (left) and 2 hours milled

556 (right) Sigmacell 20 samples.

557